Permeable Plate Anchors: Accelerating Capacity Gain in Soft Clay

C. Wang, Ph.D.[1]; C. D. O'Loughlin, Ph.D.[2]; M. F. Bransby, Ph.D.[3]; P. Watson, Ph.D.[4]; Z. Zhou, Ph.D.[5]; Y. Qi[6]; J. G. Tom, Ph.D., A.M.ASCE[7]; and S. A. Stanier, Ph.D.[8]

Abstract: Plate anchors have become an attractive technology for anchoring offshore floating facilities such as floating renewable energy devices because they provide high holding capacity relative to their dry weight. This allows for the use of smaller anchors (relative to a driven or suction-installed pile), which provide cost savings on production, transport, and installation. Loads delivered to the anchor via mooring lines may increase pore water pressure in fine-grained soils. This excess pore pressure will dissipate with time, resulting in a local increase in the undrained shear strength of the soil surrounding the anchor, increasing the capacity. There may be opportunities to consider these capacity increases if the consolidation process occurs over time periods that are short relative to the lifetime of the facility. This paper considers the use of drainage channels in a plate to make the anchor permeable and quicken consolidation times. Experimental data generated from model-scale experiments conducted in a geotechnical centrifuge show (for the anchor design tested) that excess pore pressure just above the anchor dissipated almost an order of magnitude faster for a permeable anchor, and that after full consolidation, the permeable anchor capacity was higher. The latter finding was not anticipated and is believed to be due to changes in load distribution resulting from the rapid reduction in negative excess pore pressure underneath the permeable anchor. **DOI: 10.1061/JGGEFK.GTENG-11577.**

Author keywords: Anchors and anchorages; Centrifuge modeling; Clays; Consolidation; Offshore engineering; Pore pressures.

Introduction

Moorings for offshore floating facilities require anchors embedded in the seabed to resist episodic loading from environmental events over their design life. In fine-grained soil, loads transferred by mooring lines to the anchor may generate excess pore water pressure, which will dissipate over time, leading to local increases in undrained shear strength of the surrounding soil.

Plate anchors are typically keyed after installation, with capacity (in fine-grained soils) based on undrained, unconsolidated conditions and accounting for rate and sensitivity effects where relevant. Improvements in capacity due to soil consolidation has been well demonstrated through model testing; Wong et al. (2012) and Han et al. (2016) showed capacity gains due to consolidation under monotonic loading, and Zhou et al. (2020a) described anchor capacity increases due to consolidation under combinations of sustained and cyclic loads.

Parallel experimental studies for other types of offshore foundations also provide evidence of capacity gains from soil consolidation. These studies considered axial capacity of driven piles (e.g., Doherty and Gavin 2013) and suction caissons (e.g., Jeanjean 2006), bearing capacity of shallow foundations (e.g., Randolph and Erbrich 1999; Bransby 2002), spudcan penetration resistance (e.g., Purwana et al. 2005; Bienen and Cassidy 2013), sliding resistance of mobile subsea foundations (Cocjin et al. 2014), and axial resistance of pipelines (Bruton et al. 2007; O'Beirne et al. 2021). Collectively these studies show that soil strength—and hence foundation capacity—increases if sufficient time for consolidation is permitted.

In order to bank the benefits of consolidation in design, consideration needs to be given to the time required for this process to occur. In fine-grained soils, the size of the anchor means that relatively long periods may be required to realize capacity increases—potentially longer than the time before the anchor is required in service. For plate anchors, it may be possible to accelerate the pore water dissipation time, thus advancing soil consolidation, by introducing permeable flow paths through the (normally impermeable) anchor fluke. This is similar in concept to other foundations, such as the grillage foundation (Bransby et al. 2012) and permeable piles

[1]Centre for Offshore Foundation Systems, Oceans Graduate School, Univ. of Western Australia, Perth, WA 6009, Australia. ORCID: https://orcid.org/0009-0002-1324-3565. Email: ci.wang@research.uwa.edu.au

[2]Professor, Centre for Offshore Foundation Systems, Oceans Graduate School, Univ. of Western Australia, Perth, WA 6009, Australia. Email: conleth.oloughlin@uwa.edu.au

[3]Professor, Centre for Offshore Foundation Systems, Oceans Graduate School, Univ. of Western Australia, Perth, WA 6009, Australia. Email: fraser.bransby@uwa.edu.au

[4]Professor, Centre for Offshore Foundation Systems, Oceans Graduate School, Univ. of Western Australia, Perth, WA 6009, Australia. ORCID: https://orcid.org/0000-0002-4548-8455. Email: phillip.watson@uwa.edu.au

[5]Advanced Modelling, Offshore Energy, Norwegian Geotechnical Institute, Sandakerveien 140, Oslo 0484, Norway; Centre for Offshore Foundation Systems, Oceans Graduate School, Univ. of Western Australia, Perth, WA 6009, Australia (corresponding author). ORCID: https://orcid.org/0000-0002-3575-8810. Email: zefeng.zhou@ngi.no; zefeng.zhou@uwa.edu.au

[6]Centre for Offshore Foundation Systems, Oceans Graduate School, Univ. of Western Australia, Perth, WA 6009, Australia. Email: yumeng.qi@research.uwa.edu.au

[7]US Army Engineer Research and Development Center, US Army Corps of Engineers, 3909 Halls Ferry Rd., Vicksburg, MS 39180. Email: joe.g.tom@erdc.dren.mil

[8]Geotechnical and Environmental Research Group, Univ. of Cambridge, 7a JJ Thomson Ave., Cambridge CB3 0FA, UK. ORCID: https://orcid.org/0000-0001-5671-2902. Email: sas229@cam.ac.uk

Note. This manuscript was submitted on December 21, 2022; approved on August 1, 2023; published online on October 24, 2023. Discussion period open until March 24, 2024; separate discussions must be submitted for individual papers. This paper is part of the ***Journal of Geotechnical and Geoenvironmental Engineering***, © ASCE, ISSN 1090-0241.

(Ni et al. 2017) or the use of drainage blankets beneath mudmats (Silvano et al. 2015; Watson et al. 2019).

This paper presents results from a series of centrifuge experiments that compare regular and permeable plate anchors, exploring excess pore water pressure dissipation durations and anchor capacity increases due to consolidation. Of particular interest is that the results show that not only does the introduction of flow paths lead to faster recovery, but it can also lead to enhanced capacity when compared with nonpermeable anchors.

The Permeable Plate Anchor

The permeable plate anchor aims to accelerate the dissipation of excess pore pressure around the anchor by introducing flow paths through the anchor, as shown schematically in Fig. 1(a). These flow paths enable positive excess pore pressures generated on one side of an anchor to equilibrate with negative pore pressures on the other side, thereby shortening the length of the drainage path and accelerating consolidation. Without such a shortcut of the drainage path length, equilibrium is expected to be achieved through a combination of equilibration around the perimeter of the anchor [analogous to the Osman and Randolph (2012) mechanisms for piles] and to the far field.

To explore the viability of this concept, a preliminary set of numerical analyses were conducted to model the theoretical differences in the dissipation process between an impervious and a permeable anchor. Axisymmetric finite-element analyses were conducted using Abaqus version 2010 (Dassault Systèmes 2010) to assess the consolidation rate process for a circular plate anchor with and without flow paths through the anchor body. The dimensions of the modeled axisymmetric geometry are shown in Figs. 1(a and b). The soil response in Abaqus was modeled using the Modified Cam Clay soil constitutive model (Roscoe and Burland 1968). The soil consolidation properties were assumed to correspond to a permeability $k = 4.9 \times 10^{-9}$ m/s, an effective unit weight $\gamma' = 5$ kN/m^3, and compression and swelling indices of $\lambda = 0.435$ and $\kappa = 0.044$; the anchor was modeled as a purely elastic (nonporous) material. Details of the adopted parameters are given in Table 1.

For the case of the permeable anchor, subsections of the anchor were modeled using an elastic material but with a permeability $k = 1 \times 10^{-4}$ m/s (i.e., several orders of magnitude higher than that for the clay) to allow pore water flow through the anchor and hence equilibration of excess pore pressure across the anchor. For this analysis, three porous sections were modeled within the anchor axisymmetric half-space. The dimensions and properties chosen here are somewhat arbitrary because the point of the modeling is to demonstrate in principle the differences in consolidation due to flow paths within an anchor.

Fig. 1(c) shows the results of the consolidation analysis in terms of pore pressure generation and dissipation. Figs. 1(a and b) show spatial distributions of excess pore pressure, u_e, around the solid and permeable anchors just after the load was applied and after

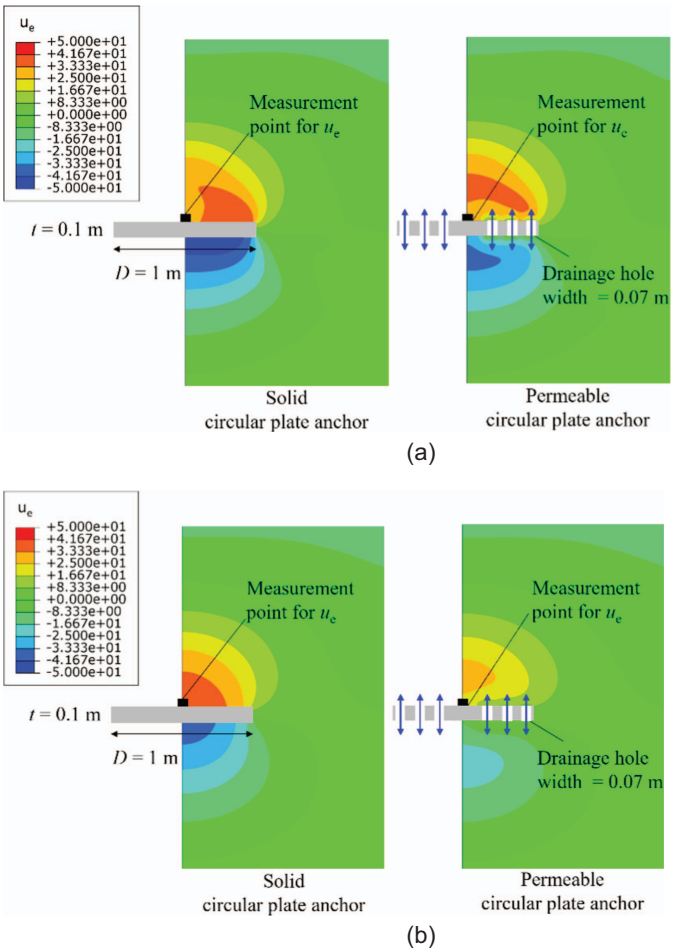

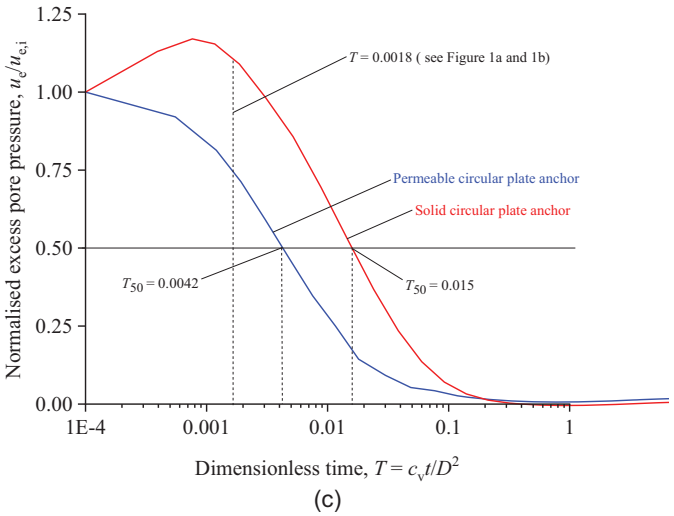

Fig. 1. (Color) Numerical simulation of consolidation for permeable and solid circular plate anchors: (a) excess pore pressure distribution at $T = 0$; (b) excess pore pressure distribution at $T = 0.0018$; and (c) evolution of excess pore pressure with time for permeable and solid anchors.

J. Geotech. Geoenviron. Eng., 2024, 150(1): 04023123

Table 1. Parameters adopted in the numerical analysis

Property	Value
Soil permeability, k (m/s)	4.9×10^{-9}
Anchor flow path permeability, k (m/s)	1.0×10^{-4}
Soil effective unit weight, γ' (kN/m^3)	5
Compression index, λ	0.435
Swelling index, κ	0.044
Poisson's ratio, ν	0.3
Stress ratio at critical state, M_q	0.92
Wet yield surface size, β	1
Flow stress ratio, K	1
Intercept on critical state line, e_{cs} (at $p' = 1$ kPa)	2.14

25% pore pressure dissipation (i.e., $u_e/u_{e,i} = 0.75$) at a position in the middle of the upper face of the anchor. The initial distribution of excess pore pressure for the solid anchor was as anticipated, with approximately equal and opposite excess pore pressures developing above and below the anchor, with the positive excess pore pressure being associated with the compressional total stress above the anchor plate and the negative excess pore pressure being associated with the tensile total stress at the base of the anchor (e.g., Han et al. 2016). In contrast, the initial distribution of excess pore pressure for the permeable anchor shows that excess pore pressure equalizes locally around the flow paths over the duration of applying the load to the anchor. Fig. 1(c) shows the evolution (dissipation) of excess pore pressure at a position in the middle of the upper face of the anchor with time.

From these results, the permeable anchor clearly indicates a faster pore pressure equilibration (and hence soil consolidation and strength gain) process. This is because positive excess pore pressures that generate above the anchor can equilibrate with (relative) negative pore pressures generated at the base of the anchor via flow through the anchor. For the solid anchors, the pore pressures must dissipate by water flowing around the perimeter of the anchor or to the far field. As a result, the calculated time to achieve approximately 50% pore pressure dissipation is 3.6 times faster for the permeable anchor.

These preliminary numerical analyses provided the motivation to explore the permeable anchor concept experimentally to evaluate the time scales over which consolidation-induced gains in anchor capacity would occur for permeable and nonpermeable anchors. These experiments are discussed in the following sections.

Experimental Program

Centrifuge model testing was performed using wished-in-place circular plate anchors in the 3.6-m-diameter beam centrifuge at the University of Western Australia's National Geotechnical Centrifuge Facility, at an acceleration level of 100g. The anchors were positioned horizontally and loaded vertically (upward) in normally consolidated clay. Individual anchor tests comprised an initial monotonic loading stage to approximately half of the anchor capacity, a consolidation pause period, and a subsequent monotonic loading stage to measure the increase in anchor capacity resulting from consolidation. One test added a cyclic loading sequence during the pause period as part of a preliminary investigation into the effect of repeated loading.

Model Anchor and Instrumentation

The circular plate anchors, one solid and one with drainage channels, are shown in Fig. 2. The solid anchors are designated as A1 in this paper, with the anchors with drainage channels referred to as A2. Each anchor is 40 mm in diameter with a 6-mm plate thickness. The anchors were fabricated from acetal (polyoxymethylene), which has an effective unit weight $\gamma' = 4.1$ kN/m^3, in an attempt to eliminate any downward self-weight pressure on the soil.

Fig. 3 shows the A2 drainage arrangement. Each A2 anchor comprises two circular plates bonded with an adhesive. The thickness of the top plate is 5 mm, and the thickness of the bottom plate is 1 mm. Drainage was achieved by cutting three circular drainage channels arranged in the four radial sections shown in Fig. 3. The drainage channels are 1.5 mm wide on the top plate and 0.5 mm wide on the bottom plate. Overall, approximately

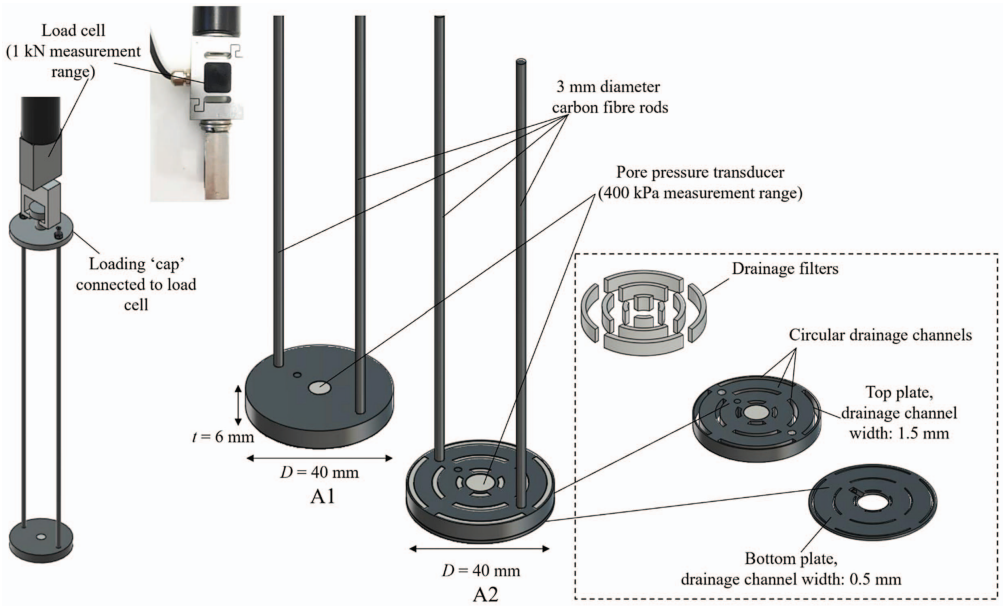

Fig. 2. (Color) Model anchors (A1 and A2) with associated instrumentation.

J. Geotech. Geoenviron. Eng., 2024, 150(1): 04023123

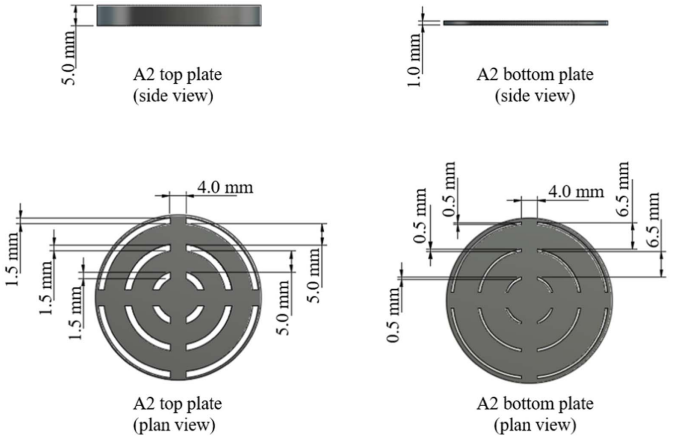

Fig. 3. Permeable plate anchor.

20% of the projected area of the anchor is taken up by drainage channels. Before testing, a 1.5-mm-thick strip of polythene drainage filter with an average pore size of 35 μm was inserted in each drainage channel on the upper plate. This was held in position by the lower plate because the drainage channel in this plate was 0.5 mm wide.

Each anchor was instrumented with a pore pressure transducer positioned in the middle of the upper side of the plate anchor. An actuator was used to load the anchors, positioned in such a way that its vertical axis was able to reach a loading cap connected to each individual anchor through two carbon fiber hollow rods with an outer diameter of 3 mm, as shown in Fig. 2. The anchor resistance was measured using a load cell located on the vertical axis of the actuator.

The entire anchor system had an equivalent total effective unit weight of approximately $\gamma' = 5.7$ kN/m^3 for the A1 anchors and $\gamma' = 5.1$ kN/m^3 for the A2 anchors, making them (approximately) neutrally buoyant in the soil ($\gamma' = \sim 5$ kN/m^3 at the initial embedment level)—thereby allowing them to be considered as wished-in-place prior to the start of testing.

Sample Preparation, Experimental Arrangement, and Soil Characterization

Sample Preparation

The tests were conducted in a normally consolidated kaolin clay (eckalite), that was mixed as a slurry with a water content of 210% (equivalent to 2.85 times the liquid limit) in a vacuum mixer for a minimum of 24 h, and then transferred to a sample container (or strongbox) with dimensions of 650 × 390 × 325 mm length × width × depth). A 25-mm sand layer overlain by a thin sheet of geofabric was placed at the base of the strongbox before adding the clay. This served as a base drain and was hydraulically connected to the surficial free water, enabling two-way drainage of the clay sample during consolidation. An initial 75-mm layer of clay slurry was placed in the strongbox and consolidated in a loading frame to a vertical stress level of 35 kPa, providing a supporting layer for the anchors to be placed upon.

Following placement of the anchors, additional slurry was added to the strongbox before it was transferred to the centrifuge. The clay was then consolidated in the centrifuge for nine days at the testing acceleration of 100g (specified at the initial depth of the anchor), with additional slurry added after 18 h to achieve a final sample height of 217 mm [Fig. 4(a)]. The lower layer of (preconsolidated) clay was free to settle during consolidation, with the anchors also allowed to move vertically. This established a normally consolidated soil state at the anchor depth because the vertical effective stress caused by the overlying clay was approximately 63 kPa (at 100g), greater than the preconsolidation stress of 35 kPa.

Experimental Arrangement

After consolidation, the anchors were located at an embedment depth of approximately 145 mm (3.63D) below the mudline, as shown in Fig. 4(a), which is sufficient for the anchor to be considered deeply embedded (e.g., Wang and O'Loughlin 2014). The final thickness of clay below the anchor was no less than 47 mm (1.15D), such that the rigid boundary was sufficiently distant for it to have minimal effect on the anchor capacity mobilization response. The minimum clear distance between individual anchors, and between anchors and the strongbox walls, was typically

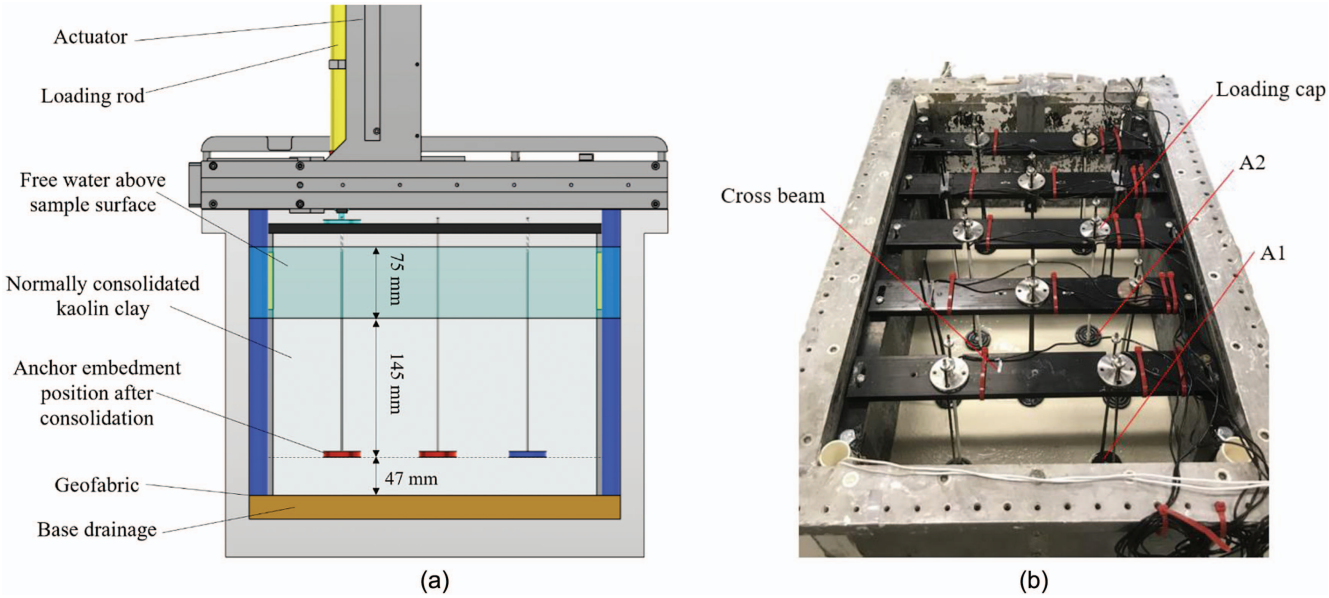

Fig. 4. (Color) Experimental arrangement: (a) end view; and (b) anchor arrangement in strongbox after consolidation of the lower clay layer.

J. Geotech. Geoenviron. Eng., 2024, 150(1): 04023123

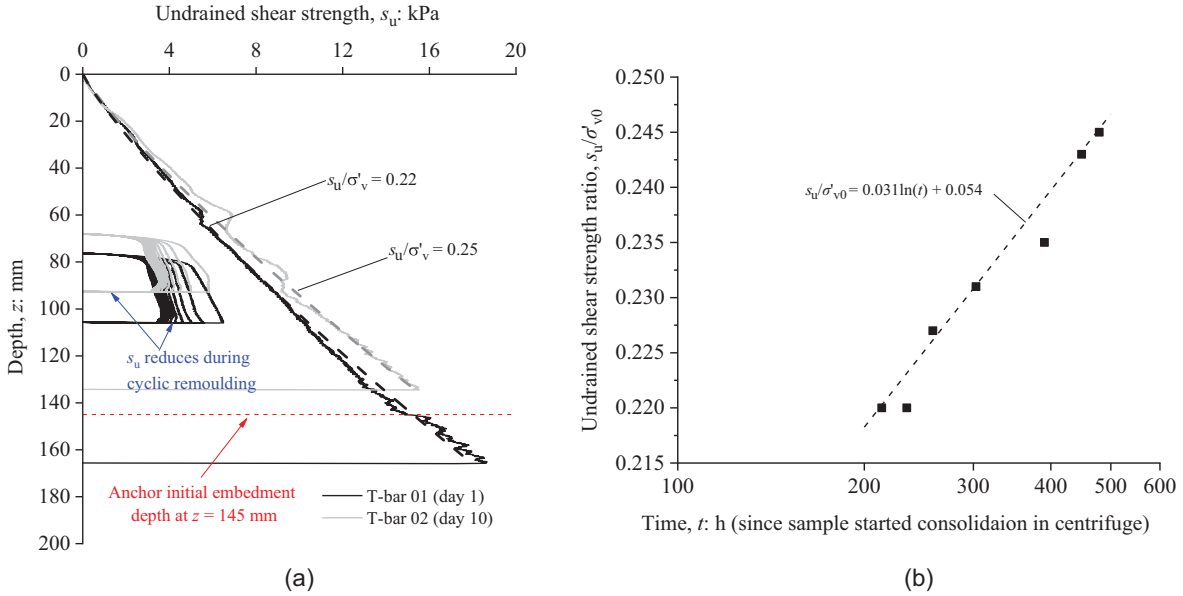

Fig. 5. (Color) Undrained shear strength from T-bar testing: (a) depth profiles; and (b) changes in undrained shear strength over time.

maintained at greater than $2.25D$ to minimize boundary effects (Zhou et al. 2020b). The arrangement of the anchors in the strongbox on the preconsolidated clay layer is shown in Fig. 4(b).

Soil Characterization

Depth profiles of intact and remoulded shear strength ($s_{u,i}$ and $s_{u,r}$, respectively) were determined from T-bar penetration tests (Stewart and Randolph 1991) conducted using a model-scale T-bar penetrometer with a diameter $d = 5$ mm and a length of 20 mm. Individual tests were performed at a velocity $v = 2$ mm/s ($V = vd/c_v = 42$, where the coefficient of vertical consolidation, $c_v = 7.5$ m^2/year, is taken at a stress level equivalent to that at the initial anchor depth), such that the response can be considered as undrained (House et al. 2001).

Fig. 5(a) shows typical undrained shear strength (s_u) profiles over the penetration depth derived from the measured penetration resistance using a T-bar factor $N_{\text{T-bar}} = 10.5$ (Martin and Randolph 2001), with an indication of the anchor depth included on the figure. It can be seen that the strength profile is linear, including in the lower (preconsolidated) clay layer.

Undrained shear strength profiles ($s_{u,i}$) are fitted by the undrained strength ratio, $s_{u,i}/\sigma'_{v0}$, which ranged from 0.22 to 0.25 over the course of 20 days of in-flight testing, and show that the sample strengthened slightly over time. These strength changes have been observed in in numerous other centrifuge studies on normally consolidated kaolin clay (e.g., Watson et al. 2000; O'Loughlin et al. 2004; Han et al. 2021), and may be associated with an apparent overconsolidation effect brought about by the numerous stop/start cycles of the centrifuge. The s_u changes were measured by performing T-bar tests in between anchor tests, with changing $s_{u,i}/\sigma'_{v0}$ plotted in Fig. 5(b) and fitted by the following logarithmic relationship:

$$s_{u,i}/\sigma'_{v0} = 0.031\ln(t) + 0.054 \quad (1)$$

where t = time since the sample started in the centrifuge. Interpretation of each anchor test involved selection of the relevant strength as per Eq. (1).

Each T-bar test included a cyclic remolding stage to determine the remolded shear strength, $s_{u,r}$, whereby the T-bar was displaced vertically by ± 15 mm ($\pm 3d$) for a total of 20 cycles, which was sufficient for the soil strength to reduce to a steady state. The soil sensitivity, S_t, was calculated as the ratio between the soil resistance measured in the initial and final penetration to give an average soil sensitivity, $S_t = s_{u,i}/s_{u,r} = 2.5$.

Test Procedure and Experiment Program

The experimental program comprised nine vertically loaded anchor tests performed to explore differences between the A1 and A2 anchors. The program of testing is summarized in Table 2, with the procedure for each anchor test described briefly as follows:

- Test 1 determined the undrained unconsolidated monotonic capacity using a solid (A1) anchor. The anchor was moved upward 40 mm ($1D$) at a velocity $v = 0.75$ mm/s such that $V = 127$ (using $c_v = 7.5$ m^2/year as noted previously) to ensure an undrained response (House et al. 2001). Both the peak and strain softened monotonic anchor capacities ($q_{uu,p}$ and $q_{uu,s}$) were obtained from this test and are considered relevant for both A1 and A2 anchors.
- For Tests 2–7 and 9, the anchor was loaded monotonically to approximately 0.42 times the normalized peak resistance established in Test 1 [accounting for changes in soil strength according to Eq. (1)], with the load sustained for various consolidation periods. The anchor was then displaced monotonically upward by approximately $1D$ using the same velocity as in Test 1.
- An exploratory test (Test 8) using a permeable (A2) anchor was performed to explore the effect of cyclic loading. In this case, the anchor was also loaded monotonically to approximately 0.42 times the normalized peak anchor resistance before applying 10 cycles of load between 0.2 and 0.6 times the normalized peak anchor resistance, after which the anchor was held at a maintained load of approximately 0.42 times the normalized peak anchor resistance for a predetermined consolidation period. A loading frequency of 0.4 Hz was chosen to strike a balance between achieving undrained conditions and high-quality load control. The anchor was then displaced monotonically at $v = 0.75$ mm/s as in the monotonic stages of the other tests.

Table 2. Summary of test program

	Initial monotonic loading			Consolidation stage			Postconsolidation monotonic loading		Dimensionless anchor resistance			
									Before consolidation		After consolidation	
Test	Anchor type	Displacement, Δz (mm)	Velocity, v (mm/s)	Control	Consolidation duration, t	Dimensionless time, $T = c_v t/D^2$	Displacement, Δz (mm)	Velocity, v (mm/s)	Normalized peak resistance, $q_{uu,p}/s_u^*$	Normalized strain softened resistance ($\Delta z = 0.5D$), $q_{uu,s}/s_u^*$	Normalized peak resistance, $q_{uu,p}/s_u^*$	Normalized strain softened resistance (between $\Delta z = 0.4D$ and $0.8D$), $q_{uu,s}/s_u^*$
1	A1	40	0.75	—	—	—	—	—	17.9	10.5	—	—
2	A1	1.2–2.0 (Δz at $q = 0.42q_{uu,p}$)		Fixed resistance, $q = 0.42q_{uu,p}$	15 h	7.85	~40 mm	0.75 mm/s	—	—	Test failed[a]	
3	A2				15 h	7.85			—	—	21.0	13.32
4	A1				7 h	3.67					19.1	10.9
5	A2				110 s	0.016					19.0	11.3
6	A1				110 s	0.016					18.0	10.58
7	A2				1,000 s	0.145					19.6	12.22
8	A2			Cyclic loading, $q = 0.2$ to $0.6\ q_{uu,p}$ for 10 cycles at a frequency of 0.4 Hz, followed by fixed resistance, $q = 0.42q_{uu,p}$	1,000 s	0.145					20.1	12.6
9	A1			Fixed resistance, $q = 0.42q_{uu,p}$	15 h	7.85					19.1	11.5

[a]Loading rod broke during second monotonic loading stage.

Results and Discussion

Anchor Undrained Unconsolidated Capacity, $q_{u,u}$

The monotonic undrained unconsolidated anchor resistance measured in Test 1 is presented in Fig. 6. The data are shown as $q_{u,u}/s_u*$ where $q_{u,u}$ is the (net) undrained unconsolidated anchor resistance and s_u^* is the strain-rate-adjusted initial undrained shear strength at the instantaneous depth of the anchor (i.e., it changes with displacement). Here, $q_{u,u}$ was determined as the measured load cell resistance minus the (estimated) rod friction and the submerged weight of the anchor/rod system, divided by the projected area of the anchor. Rod friction was calculated using the intact undrained shear strength, $s_{u,i}$, coupled with an interface friction ratio of 0.2, which gave a total rod friction that was ~4% of the measured peak anchor resistance. Also, s_u^* was adjusted from the base value given by Eq. (1) to account for the different strain rates between the anchor movement and T-bar penetration, using the commonly adopted strain-rate power law (e.g., Biscontin and Pestana 2001):

$$s_u^* = s_{u,\text{ref}} \left(\frac{v/D}{(v/d)_{\text{ref}}} \right)^n \tag{2}$$

where $s_{u,\text{ref}}$ = reference T-bar strength taken as $s_{u,i}$; n is a soil-dependent strain rate parameter, determined as $n = 0.04$ for this soil (Wang et al. 2023); $v/D = 0.019\ \text{s}^{-1}$ for the anchor tests; and $(v/d)_{\text{ref}} = 0.4\ \text{s}^{-1}$ for the T-bar tests. This leads to $s_{u,i}$ being reduced by 14% (i.e., $s_u^* = 0.86 s_{u,i}$), which is incorporated into the normalization of the anchor penetration resistance.

As shown in Fig. 6, the normalized anchor resistance, q_{uu}/s_u^*, rises to a peak value, $q_{uu,p}/s_u^* = 17.9$ after 3.9 mm (approximately $0.1D$) of anchor movement. As the anchor displaces further to approximately $0.375D$, q_{uu}/s_u^* reduces to a steady value, $q_{uu,s}/s_u^* = 10.5$, identical to $N_{\text{T-bar}} = 10.5$ used to deduce the undrained shear strength. This implies that after adjustment for strain-rate effects, the capacity factor for a T-bar and a circular plate in strain softened soil is identical, consistent with experimental observations reported by Chung et al. (2006) and with very similar recommended capacity factors for T-bar and ball penetrometers (e.g., Low et al. 2010).

The peak normalized anchor resistance, $N_c = q_{uu,p}/s_u^* = 17.9$ on Fig. 6 is much higher than exact solutions for an infinitely thin

Fig. 6. (Color) Anchor capacity mobilization response during the monotonic test (Test 1).

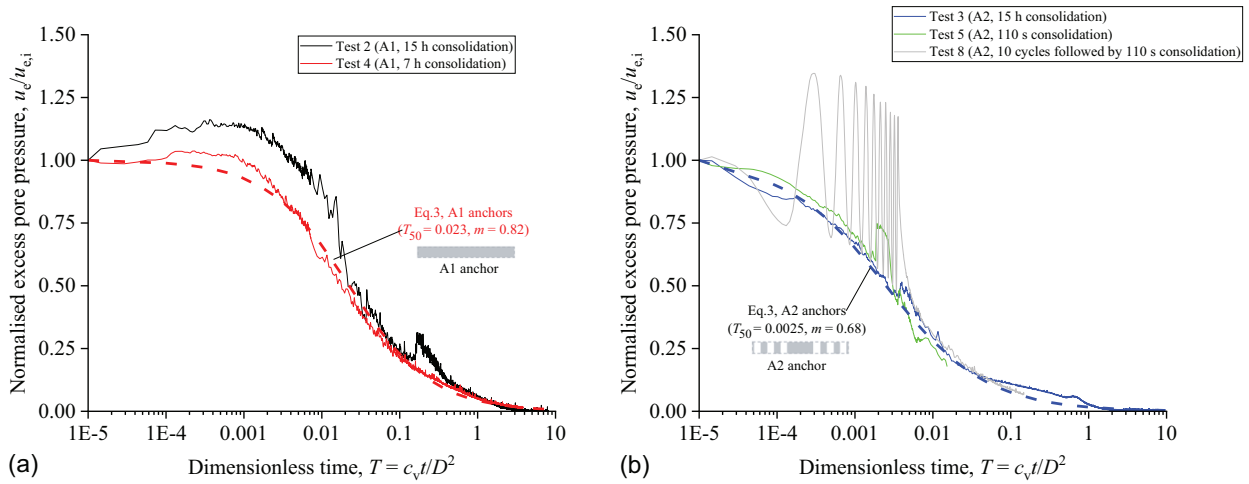

Fig. 7. (Color) Dissipation of excess pore pressure measured at the center of the upper face of (a) A1 anchor; and (b) A2 anchor.

plate, which are $N_c = 12.42$ and 13.11 for smooth and rough interfaces, respectively (Martin and Randolph 2001). Although consideration of plate thickness will increase N_c moderately (e.g., Wang and O'Loughlin 2014), the much higher experimental N_c value may be attributed to strain-rate effects that are only very slightly compensated by strain softening at such low displacement levels, or to artifacts of the experimental procedure to create wished-in place anchors.

Although not explicitly tested in this program, it was assumed that $q_{uu,p}/s_u^*$ and $q_{uu,s}/s_u^*$ for A1 and A2 anchors were identical because the inclusion of drainage in the anchor was not expected to influence the undrained resistance. Additional testing at a larger scale in the field validated this assumption (Wang 2023).

Anchor Behavior during Sustained Loading

Dissipation of Excess Pore Pressure

Fig. 7 shows the dissipation of excess pore pressure measured at the center of the top face for both the A1 [Fig. 7(a)] and A2 [Fig. 7(b)] anchors during the sustained loading stage. Excess pore pressure, u_e, on Fig. 7 is normalised by the initial excess pore pressure after reaching the maintained load, and is plotted against dimensionless time, $T = c_v t/D^2$. The excess pore pressure dissipation profiles for A1 and A2 anchors are approximated by the following hyperbolic function (DeJong and Randolph 2012):

$$\frac{u_e}{u_{e,i}} = 1 - \frac{1}{1 + (T/T_{50})^m} \tag{3}$$

where T_{50} = dimensionless time associated with 50% dissipation; and the exponent m controls the shape of the backbone dissipation curve. Eq. (3) provides good agreement with the A1 anchor [Fig. 7(a)] results using $T_{50} = 0.023$ and $m = 0.8$, whereas data from the A2 anchors [Fig. 7(b)] are best fitted using $T_{50} = 0.0025$ and $m = 0.68$. Consistent with the numerical result presented previously (Fig. 1), T_{50} reduces in response to the shortened drainage path, albeit that the reduction is much more significant in the experiments (where the reduction is a factor of 9) than in the numerical simulation (where the reduction is a factor of ~3.6) even though the spacing between the drainage channels is similar (and the parameters adopted in the numerical simulation are for the clay used in the experiments). This difference suggests that the finite-element simulation does not capture a quickening effect that is present in the experiments. This may be due to an increase in the coefficient of consolidation associated with a higher total stress above the plate (discussed subsequently).

Also evident in Fig. 7 is the Mandel-Cryer effect (e.g., Mandel 1950; Cryer 1963) for the A1 anchor, where excess pore pressure rises above the initial value of stress change during the early stage of consolidation, which is also a feature of the numerical response shown in Fig. 1. This is considered to be due to faster dissipation of excess pore pressure near the edge of the anchor than at the center of the anchor, with dissipation induced volumetric changes causing temporary transfer of the total stress toward the center of the anchor. In contrast, the Mandel-Cryer effect was not evident in either the experimental or numerical A2 anchor dissipation profiles because the excess pore pressure above the anchor was able to dissipate directly through the shorter drainage path.

Fig. 7 also shows excess pore pressure dissipation for Test 8, which included 10 loading cycles between $0.2q_{uu,p}$ and $0.6q_{uu,p}$—i.e., with a mean applied resistance of around $0.4q_{uu,p}$ as in the other tests. Additional excess pore pressure caused by the cyclic loading was evident, with u_e/u_{ei} exceeding unity in all 10 cycles in response to the peak amplitude of the applied cyclic load but reducing with T as consolidation took place. Unloading in each cycle allowed u_e/u_{ei} to reduce to the pore pressure response measured in the other A2 tests (without cyclic loading). After the 10 cycles, u_e/u_{ei} transitions to, and continues along, the monotonic dissipation curve for the A2 anchor.

Anchor Displacement

Fig. 8(a) presents vertical anchor displacement, Δz, against dimensionless consolidation time, T, during sustained loading, with $q = 0.42q_{uu,p}$. The displacement data in Fig. 8(a) suggest that the fully consolidated anchor displacement would be in the range, $\Delta z = 0.6$ to 1.1 mm, with no apparent displacement bias toward a particular anchor type. However, this interpretation ignores the increase in soil strength over the duration of the tests, which will also control soil stiffness and hence the magnitude of anchor displacement.

Fig. 8(b) plots all anchor displacements at a dimensionless time, $T = 0.01$, versus the expected soil strength at the relevant time for each test [according to Eq. (1)]. Consideration of the displacement data in this way leads to an interpretation that anchor displacements appear generally higher for the A2 anchor, suggesting that the volumetric reduction associated with consolidation of the soil above the A2 anchor is greater than for the A1 anchor. This may reflect greater total stress being applied to the soil above the A2 anchor (relative to the A1 anchor), likely leading to enhanced soil

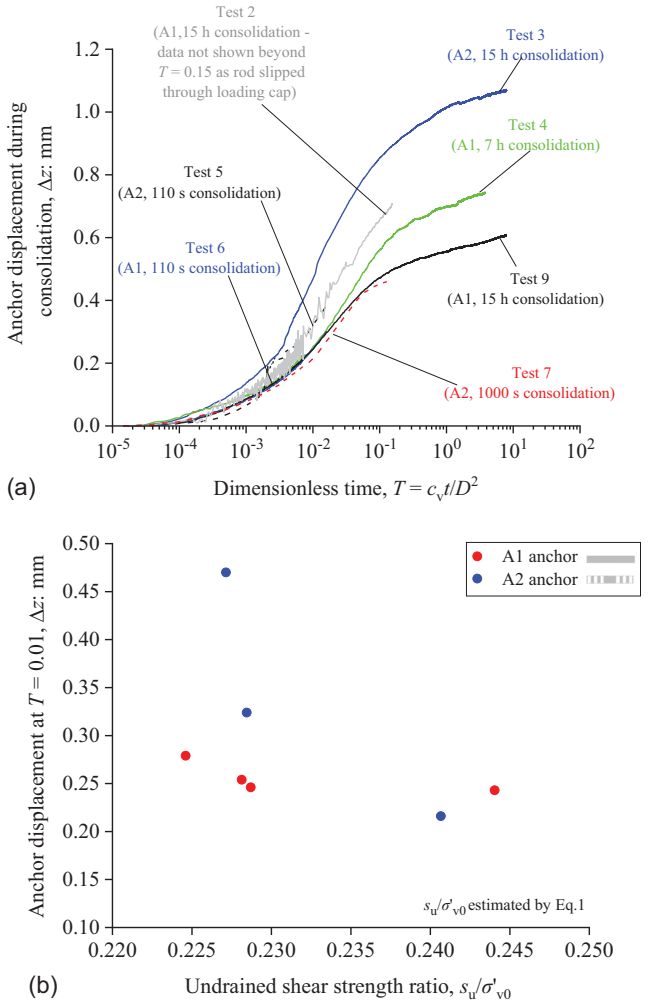

Fig. 8. (Color) Consolidated anchor displacement for A1 and A2 anchors: (a) change in anchor displacement with dimensionless time during the sustained loading stage; and (b) change in anchor displacement at $T = 0.01$ relative to the undrained shear strength ratio for each test.

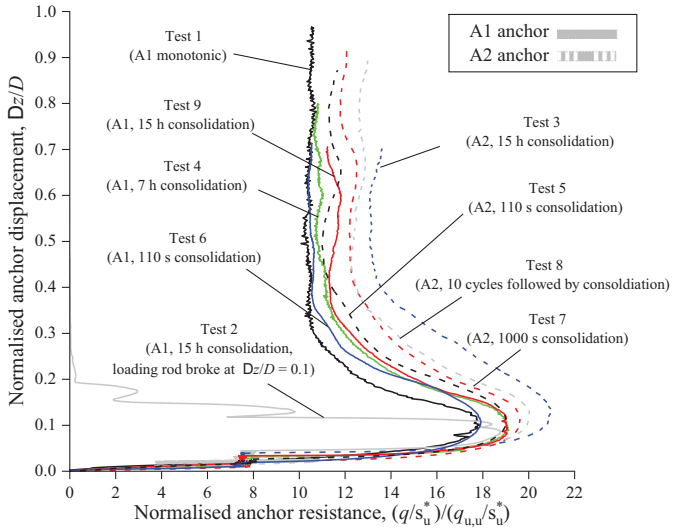

Fig. 9. (Color) Anchor capacity mobilization response after consolidation compared with that in the monotonic test (Test 1).

strength—which will become evident in the subsequent discussion. Although the A2 anchor moves marginally further than the A1 anchor when subject to the same level of sustained load, the magnitude of the displacement (for either anchor type) is negligible in the context of an anchor and mooring system, especially when considering the displacement required to key the anchor. Therefore, we believe that these minor additional movements will not limit anchor usage in general mooring systems, with the possible exception of those with exceptionally stringent displacement limits.

Anchor Consolidated Capacity

Fig. 9 shows the monotonic undrained response for both A1 and A2 anchors after sustained loading. Approximately $0.1D$ of anchor movement is required to mobilize the peak consolidated anchor resistance, $q_{cu,p}$ (arguably slightly higher for the A2 anchor), with the resistance then decreasing to a steady value, $q_{cu,s}$. Compared with the undrained unconsolidated monotonic profile (black line in Fig. 9), it is evident that consolidation causes increases in both the peak and strain-softened anchor resistance.

Fig. 10 presents the postconsolidation capacity normalized by the undrained unconsolidated capacity for both peak resistance $(q_{cu,p}/s_u^*)/(q_{uu,p}/s_u^*)$ [Fig. 10(a)] and strain-softened resistance $(q_{cu,s}/s_u^*)/(q_{uu,s}/s_u^*)$ [Fig. 10(b)]. In both cases, the response is plotted against dimensionless consolidation time (at the sustained load).

Fig. 10(a) suggests a modest increase in peak capacity of approximately 7% for the A1 anchor after full consolidation, considerably lower than the 17% measured for the A2 anchor. The results also show that the A2 anchor was able to achieve a similar peak capacity increase as the (fully consolidated) A1 anchor after maintaining the load for a period of time equal to $T = 0.016$. Also evident is the slight increase in anchor capacity when applying a modest degree of cyclic loading, which reflects an enhanced level of excess pore pressure generation during this stage as shown previously (Fig. 7).

Fig. 10(b) shows slightly higher increases in softened anchor capacity for the A2 anchor compared with the A1 anchor; the former showing 28% increase in $(q_{cu,s}/s_u^*)/(q_{uu,s}/s_u^*)$ after full consolidation compared with 11% for the A1 anchor.

Overall, the experiments demonstrate that the permeable anchor has the potential to both accelerate excess pore pressure dissipation and increase anchor capacity—the latter being an unexpected outcome from the testing, which is discussed further subsequently.

Changing Stress Field around Plate Anchors

The schematic in Fig. 11 explains the likely mechanism behind the increase in postconsolidation capacity for the A2 anchor (relative to the A1 anchor). At the start of the sustained loading stage [Fig. 11(a)], the total applied stress on the anchor, q, is anticipated to be split evenly between compression above the anchor and tension below the anchor ($\Delta\sigma_v = 0.5q$), such that there is a corresponding distribution of total stress increases and reductions above and below the anchor. This is illustrated by the Boussinesq contours (Boussinesq 1885) of total stress changes in Fig. 11(a).

As consolidation in the far-field soil commences [Fig. 11(b)], the rapid neutralization of suction beneath the A2 anchor means that the total applied stress needs to be supported totally by the soil above the anchor. This results in a greater increase in total stress in the soil above the anchor, in comparison with the A1 anchor, and so the final consolidated strength above the anchor is larger. As a result, when the anchor is subsequently loaded upward (after the stress hold), the A2 anchor moves through stronger soil than the

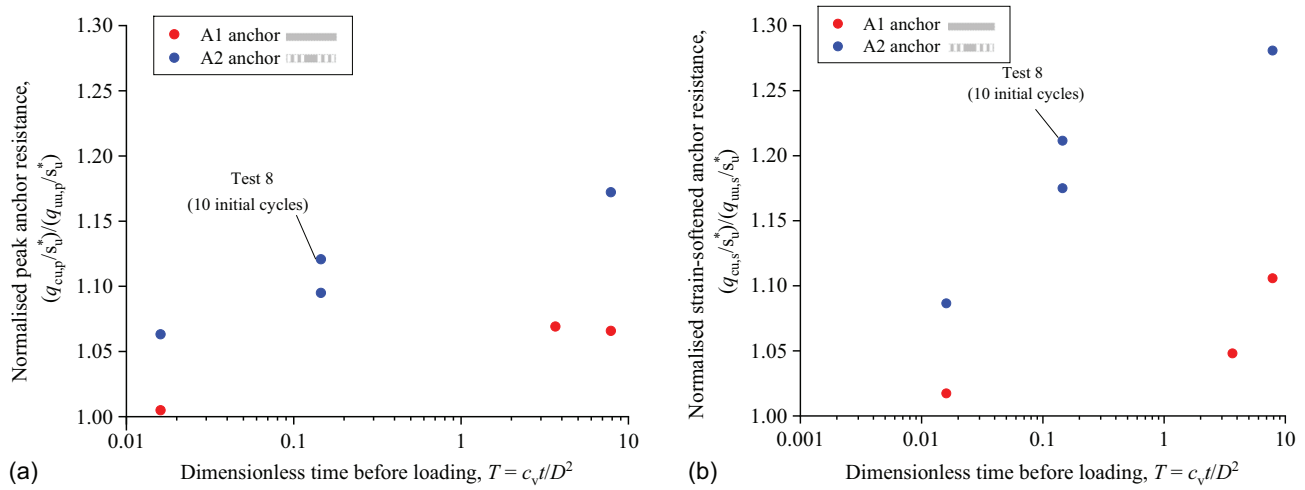

Fig. 10. (Color) Anchor capacity increases after consolidation: (a) peak capacity; and (b) average strain-softened capacity between $\Delta z = 0.4D$ and $0.8D$.

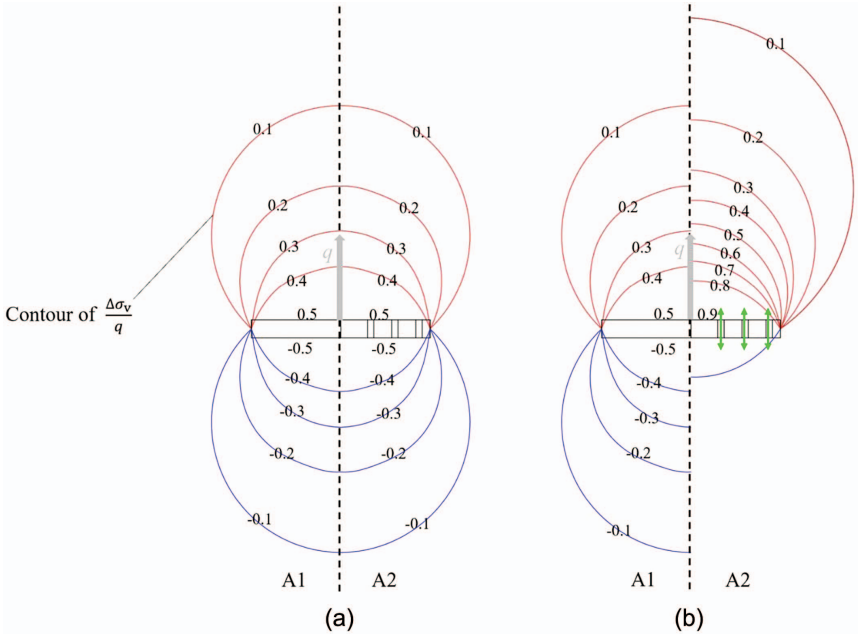

Fig. 11. (Color) Potential mechanism leading to higher A2 anchor capacity: contours of total vertical stress increase (a) at the start of consolidation; and (b) during consolidation.

A1 anchor—with the result being greater capacity gain. This remains an area for future work, to be validated either through experimental or numerical studies.

Conclusion

This paper described a set of centrifuge experiments that have explored the benefit of introducing permeable sections in plate anchors to reduce the time required to achieve benefits related to consolidation under both maintained and cyclic loading. The permeable anchor tested here facilitated dissipation of excess pore pressure (at a central location on the upper face of the plate) nine times faster than its counterpart impermeable anchor, with a subsequent postconsolidated peak anchor capacity that was 17% higher than that without consolidation, compared with a 7% increase for the impermeable anchor. Although only tested for one anchor geometry, it appears that low levels of cyclic loading lead to further enhancements in capacity above that seen for the permeable anchor only.

A typically sized plate anchor measuring 10 m in length and 4.5 m in height (Brown et al. 2010) installed in soil with a c_v of 1 to 10 m^2/year would take 0.6 to 6 years to reach 90% consolidation (assuming a dimensionless period, $T = tc_v/B^2 = 0.3$, Zhou et al. 2020b). The results presented here indicate that a permeable anchor could reduce consolidation time for this anchor from 7 months to 1 month for $c_v = 10$ m^2/year, and from 6 years to 8 months for $c_v = 1$ m^2/year, allowing for a significant increase in anchor capacity prior to operational loading. Hence, the ability to reduce consolidation time could allow the associated higher soil

strength to be utilized over practical time scales. This provides for opportunities to achieve a design capacity with a smaller anchor, reducing installation costs, or to increase safety margins through the lifetime of the mooring system. Such anchors could be used in future renewable energy developments to provide increased efficiency with respect to capacity and time from installation to operation.

Data Availability Statement

Some or all data, models, or code that support the findings of this study are available from the corresponding author upon reasonable request.

Acknowledgments

The first author acknowledges her research studentship from the University of Western Australia. This work was supported by the ARC Industrial Transformation Research Hub for Offshore Floating Facilities which is funded by the Australia Research Council, Woodside Energy, Shell, Bureau Veritas, and Lloyds Register (Grant No. IH140100012). The third author acknowledges the support of Fugro, provided via the Fugro Chair in Geotechnics at UWA. The fourth author leads the Shell Chair in Offshore Engineering research team at the University of Western Australia, which is sponsored by Shell Australia. The corresponding author acknowledges support from the Norwegian Geotechnical Institute (NGI).

Notation

The following symbols are used in this paper:

c_v = coefficient of vertical consolidation;
D = plate diameter;
d = T-bar diameter;
e = voids ratio;
e_{cs} = intercept on critical state line;
K = flow stress ratio;
k = permeability;
M_q = stress ratio at critical state;
m = parameter for dissipation rate;
N_c = anchor capacity factor;
$N_{\text{T-bar}}$ = T-bar factor;
n = strain rate parameter;
p' = mean effective stress;
q = anchor resistance;
$q_{c,u}$ = consolidated undrained anchor resistance;
$q_{cu,p}$ = peak consolidated anchor capacity;
$q_{cu,s}$ = strain-softened consolidated anchor capacity;
$q_{u,u}$ = undrained unconsolidated anchor resistance;
$q_{uu,p}$ = peak undrained unconsolidated anchor resistance;
$q_{uu,s}$ = strain-softened undrained unconsolidated anchor resistance;
S_t = soil sensitivity;
s_u = undrained shear strength;
s_u^* = strain rate adjusted initial undrained strength;
$s_{u,i}$ = initial undrained shear strength;
$s_{u,r}$ = remolded undrained shear strength;
$s_{u,\text{ref}}$ = reference T-bar strength (taken as $s_{u,i}$);
T = dimensionless time;
T_{50} = dimensionless time associated with 50% consolidation;
t = time;
U = degree of consolidation;
u_e = excess pore pressure;
$u_{e,i}$ = initial excess pore pressure;
V = dimensionless velocity;
v = velocity;
z = depth;
β = wet yield surface size;
γ' = effective unit weight of soil;
Δz = anchor displacement;
$\Delta\sigma_v$ = change in total stress (maintained load);
κ = recompression index;
λ = version compression index;
ν = Poisson's ratio; and
σ'_{v0} = initial vertical effective stress.

References

Bienen, B., and M. J. Cassidy. 2013. "Set up and resulting punch-through risk of jack-up spudcans during installation." *J. Geotech. Geoenviron. Eng.* 139 (12): 2048–2059. https://doi.org/10.1061/(ASCE)GT.1943-5606.0000943.

Biscontin, G., and J. M. Pestana. 2001. "Influence of peripheral velocity on vane shear strength of an artificial clay." *Geotech. Test. J.* 24 (4): 423–429. https://doi.org/10.1520/GTJ11140J.

Boussinesq, J. 1885. *Application des potentiels à l'étude de l'équilibre et du mouvement des solides élastiques: Mémoire suivi de notes étendues sur divers points de physique mathématique et d'analyse*. [In French.] Paris: Gauthier-Villars.

Bransby, M. F. 2002. "The undrained inclined load capacity of shallow foundations after consolidation under vertical loads." In *Proc., 8th Int. Symp. on Numerical Models in Geomechanics (NUMOG)*, 431–437. Perth, Australia: Univ. of Western Australia. https://doi.org/10.1201/9781439833797-c63.

Bransby, M. F., J. A. Knappett, M. J. Brown, and P. Hudacsek. 2012. "The vertical capacity of grillage foundations." *Géotechnique* 62 (3): 201–211. https://doi.org/10.1680/geot.9.P.131.

Brown, R. P., P. C. Wong, and J. M. Audibert. 2010. "SEPLA keying prediction method based on full-scale offshore tests." In *Proc., 2nd Int. Symp. on the Frontiers in Offshore Geotechnics*. London: Taylor and Francis Group.

Bruton, D., M. Carr, and D. J. White. 2007. "The influence of pipe-soil interaction on lateral buckling and walking of pipelines: The SAFEBUCK JIP." In *Proc., 6th Int. Conf. Offshore Site Investigation Geotechnics*, 133–150. London: Society for Underwater Technology.

Chung, S. F., M. F. Randolph, and J. A. Schneider. 2006. "Effect of penetration rate on penetrometer resistance in clay." *J. Geotech. Geoenviron. Eng.* 132 (9): 1188–1196. https://doi.org/10.1061/(ASCE)1090-0241(2006)132:9(1188).

Cocjin, M. L., S. M. Gourvenec, D. J. White, and M. F. Randolph. 2014. "Tolerably mobile subsea foundations-observations of performance." *Géotechnique* 64 (11): 895–909. https://doi.org/10.1680/geot.14.P.098.

Cryer, C. W. A. 1963. "A comparison of the three-dimensional consolidation theories of Biot and Terzaghi." *Q. J. Mech. Appl. Math.* 16 (4): 401–412. https://doi.org/10.1093/qjmam/16.4.401.

Dassault Systèmes. 2010. *ABAQUS analysis users' manual*. Providence, RI: Simula.

DeJong, J. T., and M. Randolph. 2012. "Influence of partial consolidation during cone penetration on estimated soil behavior type and pore pressure dissipation measurements." *J. Geotech. Geoenviron. Eng.* 138 (7): 777–788. https://doi.org/10.1061/(ASCE)GT.1943-5606.0000646.

Doherty, P., and K. Gavin. 2013. "Pile aging in cohesive soils." *J. Geotech. Geoenviron. Eng.* 139 (9): 1620–1624. https://doi.org/10.1061/(ASCE)GT.1943-5606.0000884.

Han, C., D. Wang, C. Gaudin, C. O'Loughlin, and M. J. Cassidy. 2021. "Capacity of plate anchors in clay under sustained uplift." *Ocean Eng.* 226 (Apr): 108799. https://doi.org/10.1016/j.oceaneng.2021.108799.

Han, C., D. Wang, C. Gaudin, C. D. O'Loughlin, and M. J. Cassidy. 2016. "Behaviour of vertically loaded plate anchors under sustained uplift." *Géotechnique* 66 (8): 681–693. https://doi.org/10.1680/jgeot.15.P.232.

House, A. R., J. R. M. S. Olivera, and M. F. Randolph. 2001. "Evaluating the coefficient of consolidation using penetration tests." *Int. J. Phys. Modell. Geotech.* 1 (3): 17–26. https://doi.org/10.1680/ijpmg.2001.010302.

Jeanjean, P. 2006. "Setup characteristics of suction anchors for soft Gulf of Mexico clays: Experience from field installation and retrieval." In *Proc., Offshore Technology Conf.* Houston: IOS Press.

Low, H. E., T. Lunne, K. H. Andersen, M. A. Sjursen, X. Li, and M. F. Randolph. 2010. "Estimation of intact and remoulded undrained shear strengths from penetration tests in soft clays." *Géotechnique* 60 (11): 843–859. https://doi.org/10.1680/geot.9.P.017.

Mandel, J. 1950. "Étude mathématique de la consolidation des sols." [In French.] In Vol. 4 of *Proc., Actes du Colloque International de Méchanique*, edited by P. Vernotte, 9–19. Paris: Ministère de l'Air.

Martin, C. M., and M. F. Randolph. 2001. "Application of the lower bound and upper bound theorems of plasticity to collapse of circular foundation." In Vol. 2 of *Computer methods and advances in geomechanics*, edited by C. Desai, T. Kundu, S. Harpalani, D. Contractor, and J. Kemeny, 1417–1428. Boca Raton, FL: CRC Press.

Ni, P., S. Mangalathu, G. Mei, and Y. Zhao. 2017. "Laboratory investigation of pore pressure dissipation in clay around permeable piles." *Can. Geotech. J.* 55 (9): 1257–1267. https://doi.org/10.1139/cgj-2017-0180.

O'Beirne, C., P. Watson, C. O'Loughlin, D. White, A. Hodson, S.-Y. Ang, S. Frankenmolen, J. Hoj-Hansen, M. Kuo, and T. Roe. 2021. "Pipe clamping mattresses to mitigate flowline walking; Physical modelling trials on three offshore soils." In *Proc., Offshore Technology Conf.* Houston: OnePetro.

O'Loughlin, C. D., M. F. Randolph, and M. Richardson. 2004. "Experimental and theoretical studies of deep penetrating anchors." In *Proc., Offshore Technology Conf.* Houston: OnePetro.

Osman, A. S., and M. F. Randolph. 2012. "Analytical solution for the consolidation around a laterally loaded pile." *Int. J. Geomech.* 12 (3): 199–208. https://doi.org/10.1061/(ASCE)GM.1943-5622.0000123.

Purwana, O. A., C. F. Leung, Y. K. Chow, and K. S. Foo. 2005. "Influence of base suction on extraction of jack-up spudcans." *Géotechnique* 55 (10): 741–753. https://doi.org/10.1680/geot.2005.55.10.741.

Randolph, M., and C. Erbrich. 1999. "Design of shallow foundations for calcareous sediments." In *Proc., 2nd Int. Conf. on Engineering for Calcareous Sediments, Bahrain*. San Francisco: Environmental Science Associates.

Roscoe, K. H., and J. B. Burland. 1968. "On the generalised stress-strain behaviour of 'wet clay'." In *Engineering plasticity*, 535–609. Cambridge, UK: Cambridge University Press.

Silvano, R., C. Jaeck, H. Versteele, A. Longuet, and D. Bignold. 2015. "Stability assessment of A-shaped mudmats of mobile production units." In *Proc., Frontiers in Offshore Geotechnics III: Proc. of the 3rd Int. Symp. on Frontiers in Offshore Geotechnics (ISFOG 2015)*. London: Taylor and Francis Group.

Stewart, D. P., and M. F. Randolph. 1991. "A new site investigation tool for the centrifuge." In *Proc., Int. Conf. on Centrifuge Modelling (Centrifuge 91)*, 531–538. Boulder, CO: IOS Press.

Wang, C. 2023. "Realising 'whole-life' soil strength changes in the capacity of offshore plate anchors." Ph.D. thesis, Ocean Graduate School, Univ. of Western Australia.

Wang, C., C. D. O'Loughlin, M. F. Bransby, P. Watson, and Z. Zhou. 2023. "Time-dependent processes influencing offshore foundations in clay: An experimental study on plate anchors." *Géotechnique*.

Wang, D., and C. D. O'Loughlin. 2014. "Numerical study of pull-out capacities of dynamically embedded plate anchors." *Can. Geotech. J.* 51 (11): 1263–1272. https://doi.org/10.1139/cgj-2013-0485.

Watson, P. G., et al. 2019. "Foundation design in offshore carbonate sediments-building on knowledge to address future challenges." In *Proc., 16th Pan-American Regional Conf. on Soil Mechanics and Geotechnical Engineering*, 240–274. Cancun, Mexico: IOS Press.

Watson, P. G., M. F. Randolph, and M. F. Bransby. 2000. "Combined lateral and vertical loading of caisson foundations." In *Proc., Offshore Technology Conf.* Houston: OnePetro.

Wong, P., C. Gaudin, M. Randolph, M. Cassidy, and Y. Tian. 2012. "Performance of suction embedded plate anchors in permanent mooring applications." In *Proc., 22nd Int. Offshore and Polar Engineering Conf.*, 640–645 Houston: OnePetro.

Zhou, Z., C. D. O'Loughlin, D. J. White, and S. A. Stanier. 2020a. "Improvements in plate anchor capacity due to cyclic and maintained loads combined with consolidation." *Géotechnique* 70 (8): 732–749. https://doi.org/10.1680/jgeot.19.TI.028.

Zhou, Z., D. J. White, and C. D. O'Loughlin. 2020b. "The changing strength of carbonate silt: Parallel penetrometer and foundation tests with cyclic loading and reconsolidation periods." *Can. Geotech. J.* 57 (11): 1664–1683. https://doi.org/10.1139/cgj-2019-0066.